# Pulsed octupole magnet for beam instability mitigation in Rapid Cycling Synchrotron*

Liang-Sheng Huang,[1,2,3,†] Shou-Yan Xu,[1,2] Yun-Tao Liu,[1,2] Yi-Qin Liu,[1,2] Jian-Liang Chen,[1,2] Chang-Dong Deng,[1,2] Ming-Yang Huang,[1,2] Li Rao,[1,2,3] Han-Yang Liu,[1,2] and Xin Qi[1,2,3,‡]

[1] *Spallation Neutron Source Science Center, Dongguan, 523803, China*
[2] *Institute of High Energy Physics, CAS, Beijing, 100049, China*
[3] *University of Chinese Academy of Sciences, Beijing 100049, China*

The Rapid Cycling Synchrotron (RCS) in the China Spallation Neutron Source (CSNS) operates as a high-intensity proton accelerator. The coupled bunch instability was observed during the RCS beam commissioning, which highly limits the beam power. To investigate the dynamics of instability under increased beam power, a pulsed octupole magnet with a gradient of $900\,\mathrm{T}/m^3$ is developed. The magnet system integrates an octupole magnet with a pulsed power supply. The field is carefully measured to examine the performance before installation into the tunnel. After the installation of the magnets, beam measurements are performed to confirm the effectiveness of the instability mitigation on an actual proton beam. The measurement results show that the instability can be suppressed by using the pulsed octupole magnet, particularly at the high energy stage in an acceleration cycle, meeting the requirements for stable operation of the accelerator. Additionally, when the instability is completely suppressed through chromaticity optimization, octupole magnets can significantly enhance the RCS transmission efficiency, which is crucial for controlling beam loss. The pulsed octupole magnet offers significant progress of beam stability in the RCS, providing valuable experience for further beam power enhancement.

Keywords: China spallation neutron source, rapid cycling synchrotron, coupled bunch instability, octupole magnet

## I. INTRODUCTION

Octupole magnets have been extensively employed in ring accelerators to cure transverse instabilities, as evidenced by their application in various facilities including the photon factory electron storage ring at KEK [1] and the main ring at J-PARC [2] in Japan, LHC [3] at CERN in Switzerland, SIS100 synchrotron [4] in Germany and BEPC [5] in China. The tune spread increases with octupole field strength, thereby enhancing Landau damping. However, due to the nonlinear feature of the field, the octupole magnet will reduce the dynamic aperture [6], which restricts their power. Consequently, although instabilities have been successfully controlled [1, 2, 5], some accelerators, exemplified by the J-PARC main ring [2], faced beam loss resulting from a reduced dynamic aperture post-instability suppression. Furthermore, the nonlinear dynamics of octupole magnets become increasingly complex under the influence of space charge effects, which may reduce the efficacy of Landau damping. Therefore, a comprehensive understanding of the application of octupole magnets for mitigating instabilities is crucial for the proton Rapid Cycling Synchrotron (RCS), where the magnetic field changes rapidly and the beam size is relatively large [2, 7, 8].

The China Spallation Neutron Source (CSNS) [9, 10] is a high-intensity proton accelerator-based facility. The accelerator complex comprises two main parts: a Negative Hydrogen ($\mathrm{H}^-$) Linac [11–13] and a RCS [7, 14]. The RCS is a four-fold structure lattice with the circumference of $227.92$ meters, including 24 dipole magnets and 48 quadrupole magnets. Each super-period of the RCS consists of a straight section and an arc section. The RCS accelerates the proton beam from $80\,\mathrm{MeV}$ to $1.6\,\mathrm{GeV}$ at a repetition rate of $25\,\mathrm{Hz}$. The designed beam power of CSNS is $100\,\mathrm{kW}$, corresponding to particles of $N_p = 1.56 \times 10^{13}$ per pulse. Beam commissioning of the RCS started in 2017. An unforeseen instability in the horizontal plane was first observed [15, 16], which has emerged as a critical challenge during beam commissioning. A series of measurements provided valuable insights and practical guidance for the instability mitigation. After two years of beam commissioning and gradual power ramp-up, the RCS achieved the target beam power of $100\,\mathrm{kW}$ in February, 2020. Currently, with the aid of AC sextupole magnets [17], trim quadrupole magnets [18] and $2^{nd}$ harmonic cavities [19, 20], the beam power in the RCS has been increased to $170\,\mathrm{kW}$, corresponding to $N_p = 2.65 \times 10^{13}$ particles per pulse. In Phase II of CSNS (CSNS-II) [21], the beam power on the target will be upgraded to $500\,\mathrm{kW}$, while the energy on the target will remain unchanged (the RCS injection energy will be increased to $300\,\mathrm{MeV}$ to mitigate space charge effects). This implies a substantial increase in the beam intensity (equivalent to a particle number of $N_p = 7.8 \times 10^{13}$ per pulse). As the RCS beam intensity increases, the high-intensity effects become more serious. Notably, the instability observed during the beam commissioning at CSNS presents a significant challenge for complete suppression at CSNS-II.

We investigated the potential of employing an octupole magnet to address instability in the RCS, so a pulsed octupole magnet was proposed and developed in 2022. Following careful field measurements, the magnet system was seamlessly integrated into the accelerator in the summer of 2023. In subsequent machine studies until now, extensive beam experiments were conducted, including magnetic field calibrations and validation of instability suppression. These experiments gave several positive results for suppressing instabil-

* Supported by the Guangdong Basic and Applied Basic Research Foundation, China (Project: 2021B1515140007)
† Corresponding author, huangls@ihep.ac.cn
‡ Corresponding author, qix@ihep.ac.cn

ity, demonstrating the feasibility of using octupole magnets to mitigate instabilities in the RCS of CSNS.

This paper starts with a summary of RCS instabilities in Sec. II, highlighting the requirement for octupole magnets in suppressing the instability, as discussed in Sec. III. Sec. IV introduces the design of the magnet and its power supply, as well as the magnetic field measurements in Sec. V. Sec. VI presents beam measurements for instability mitigation. Detailed discussions on the application of octupole magnets in the RCS are provided in Sec. VII, followed by a summary in the concluding section.

## II. BEAM INSTABILITY IN THE RCS

An unexpected instability was observed during the increase of beam power from 20 kW to 50 kW in 2019, worsening with further increases in beam power. A series of comprehensive measurements [22] were undertaken to characterize the instability during a typical acceleration cycle, revealing that the issue is a coupled bunch instability. When the instability occurs, an oscillation of the beam position is observed in the transverse plane. The instability exhibits sensitivity to the tune, as illustrated in Fig. 3 of Ref. [23]. Variations in the tune lead to corresponding shifts in the timing of instability occurrences. We take the case of $\nu_x = 4.80$ as an example, as shown in Fig. 1, where the turn-by-turn (TbT) beam position in the horizontal plane and transmission efficiency in the RCS dependence on the beam population are presented. Starting from the lowest bunch intensity, the horizontal beam position begins to oscillate after injection. The oscillation amplitude becomes larger as beam intensity increases. The centroid's positive envelope on a logarithmic scale is linearly fitted, and the growth time is provided. For the beam intensity of $N_p = 1.56 \times 10^{13}$ per pulse, equivalent to a beam power of 100 kW, the growth time is less than 1 ms. In the experiment, only the coupled mode of one is determined for the normal bunch mode (two bunches). The instability is first observed in the horizontal plane and subsequently may appear in the vertical plane as the beam power increases at $\nu_y > 4.86$. The coupled mode of the vertical instability is the same with that in the horizontal plane. The impedance study confirms that the instability is induced by a resonant impedance from the RF shield on the ceramic chamber [23, 24].

Comprehensive measurements provide valuable insights and practical guidance for mitigating the instability, such as tune and chromaticity optimization. By applying the optimized tune and chromaticity, the instability has been successfully suppressed at a beam power of 100 kW [15]. Following the beam commissioning, the designed DC sextupole field was upgraded to an AC sextupole field [17]. This upgrade allows for dynamic control of chromaticity over the entire acceleration cycle, thereby enhancing beam transmission efficiency and suppressing instability simultaneously. Consequently, the RCS transmission efficiency was significantly improved, and instabilities were fully mitigated at a beam power of 170 kW.

Although the optimization of tune and chromaticity has been successfully implemented in the RCS, observations indicate that the beam power, using these two mitigation methods, reaches the threshold of instability. The approved upgrade of CSNS-II aims to increase beam power to 500 kW by increasing the particle numbers in the RCS over the forthcoming years, which poses challenges for instability mitigation. Therefore, further studies are necessary to understand the dynamic of instability under increased beam power, including proposing new and effective mitigation strategies to ensure the designed beam power. Given their critical role in mitigating collective instabilities in numerous hadron synchrotrons [2–4], octupole magnets are a primary option in the RCS of the CSNS.

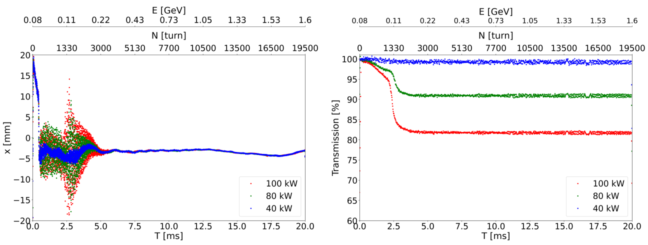


Fig. 1. (Color online) TbT beam position in the horizontal plane (left) and RCS beam transmission efficiency (right) vary with beam intensity under tune of (4.80, 4.86) with natural chromaticity. Red, green, and blue dots correspond to beam populations of $1.56 \times 10^{13}$, $1.25 \times 10^{13}$ and $0.62 \times 10^{13}$ per pulse, respectively.

## III. REQUIREMENT OF OCTUPOLE FILED FOR THE INSTABILITY MITIGATION

Based on the classical calculation of the tune shift [25], the magnetic field of an octupole magnet in accelerators can be formulated as

$$B_y + iB_x = K_3(x + iy)^3, \quad (1)$$

where, $B_x$ and $B_y$ represent the horizontal (x) and vertical (y) magnetic fields, respectively. For the particle rigidity $B\rho$ with a magnet length $l$, the octupole integrated strength is given by

$$K_3 = \frac{1}{6}\frac{k_3 l}{B\rho}, \quad (2)$$

with

$$k_3 = \frac{\partial^3 B_y}{\partial x^3}. \quad (3)$$

The horizontal and vertical magnetic fields in Eq. (1) are written as

$$B_x = K_3(3x^2 y - y^3), \quad (4)$$

$$B_y = K_3(x^3 - 3xy^2). \quad (5)$$

Octupole magnets are utilized to control the tune shift in

the transverse plane. Under reasonable simplifications [1, 26], the horizontal and vertical amplitude-dependent tune shifts are described as

$$\Delta Q_x = \frac{3}{8\pi} J_x \sum_i \beta_{x,i}^2 K_{3,i} - \frac{3}{4\pi} J_y \sum_i \beta_{x,i}\beta_{y,i} K_{3,i}, \quad (6)$$

$$\Delta Q_y = \frac{3}{8\pi} J_y \sum_i \beta_{y,i}^2 K_{3,i} - \frac{3}{4\pi} J_x \sum_i \beta_{x,i}\beta_{y,i} K_{3,i}, \quad (7)$$

where, the summation represents the sum across all magnets with indexed by $i$. $\beta_x$ and $\beta_y$ are horizontal and vertical betatron functions, respectively. $J_x$ and $J_y$ denote actions in transverse plane, with their average value related to the beam emittance $\epsilon$ by $2 < J >= \epsilon$. As indicated by Eqs. (6) and (7), the amplitude-dependent tune shifts are likely linear functions of the octupole field strength. For an example estimation in the RCS of CSNS, let us assume four octupole magnets of identical strength $K_3$, with $\beta_x = \beta_y = 8$ m at magnets locations and $J_x \approx J_y = 30$ $\pi$·mm·mrad, the tune shift is

$$\Delta Q_x = \Delta Q_y = -7 \times 10^{-4} \cdot K_3. \quad (8)$$

The required root mean square (RMS) frequency spread $\Delta\omega$ to suppress this instability can be expressed as [27]

$$\Delta\omega \geq (\Delta\omega)_{\mathrm{dyn}} \cdot \sqrt{\pi/2}, \quad (9)$$

with the dynamic part of the wake-induced betatron frequency shift $(\Delta\omega)_{\mathrm{dyn}}$, which relates to the growth time $\tau$ [28] of $(\Delta\omega)_{\mathrm{dyn}} = 1/\tau$. The growth time is assumed to be $0.5\,\mathrm{ms}$ and the required frequency spread for suppressing instability $\Delta\omega \geq 2.5 \times 10^3$ Hz. This implies the tune shift must be greater than 0.005, requiring an integrated octupole field strength of $K_3 \approx 7$ T/$m^2$ to effectively mitigate the instability.

To further investigate the efficacy of the octupole field in mitigating instability, we conducted 6D macroparticle tracking simulations using the existing code [29], which includes a representation of a single octupole magnet. A resonant wake from ceramic chambers, as detailed in TBALE 1, is employed. The simplified physical model for the interaction between the beam and the wake field accumulates the wake force into a kick momentum. Macroparticles experience the wake field effects at the interaction points in each revolution. To track particle dynamics with energy ramping, the transfer matrix of synchrotron motion is included in the simulation. The tune shift caused by the octupole field is related to the transverse amplitude. The painting process in the RCS has been included in the simulation, which makes the beam distribution closed to the realistic one. The TbT beam position oscillation with varying octupole strengths is displayed in Fig. 2, clearly showing a reduction in oscillation amplitude as octupole strength increases. Two tunes, displaying the observed instability over acceleration cycle, are simulated at a beam power of 100 kW. The results clearly demonstrate the mitigating effect of the octupole field. Additionally, the simulation indicates an additional beam loss in the presence of the octupole field after mitigating instability during the acceleration cycle. Therefore, the octupole magnetic field should be rapidly reduced to minimize beam loss.

TABLE 1. Main parameters used in simulation.

| Parameter [unit] | Value |
|---|---|
| Bunch number | 2 |
| Beam power [kW] | 100 |
| Beam energy [GeV] | 0.08 - 1.6 |
| Res. impedance $R_s$ [MΩ/m] | 1 |
| Res. frequency $f_r$ [MHz] | 0.12 |
| Quality factor $Q$ | 40 |
| Wake decay time [turns] | 500 |
| Number of macroparticles | $1 \times 10^4$ |

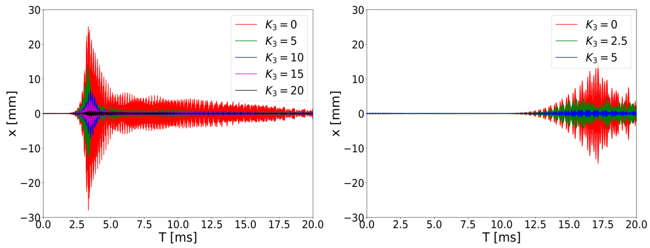


Fig. 2. (Color online) Simulated TbT beam position with the resonant wake in TABLE 1 in term of octupole field strength, where the beam power is 100 kW at tunes of $\nu_x = 4.80$ (left) and $\nu_x = 4.90$ (right), respectively.

## IV. DESIGN OF PULSED OCTUPOLE MAGNET

To dynamically control the tune spread over an acceleration cycle and minimize beam loss in the RCS, a pulsed octupole magnet is proposed. The required field gradient of the pulsed octupole magnet is related to the betatron function at the octupole magnet. To mitigate the effects of eddy current and ohmic losses [30], ceramic chambers must be utilized. These chambers are already employed in dipoles, quadrupoles, and injection painting magnets in the RCS with not much free space. The lattice in the RCS employs a triplet structure with four-fold symmetry [7]. This design effectively mitigates the effects of low-order structural resonances. In addition, the existing magnets, including sextupole magnets [17], trim quadrupole magnets [18] and correctors [31], have successfully maintained this symmetry. Consequently, four octupole magnets are suggested. The location near quadrupoles QF06 in every super-period, as shown in Fig. 3, is chosen to accommodate the octupole magnets. This choice not only preserves the symmetry of the lattice but also effectively utilizes the available ceramic chambers. At the location of octupole magnets, the horizontal and vertical betatron functions are 8.3 m and 8.0 m, respectively. According to the calculations in Fig. 2, $K_3$ is determined to be 20 T/m$^2$ at the low energy stage. Considering a beam power of 500 kW at CSNS-II, the target $K_3$ value should be close to 100 T/m$^2$. As the

energy increases, the required strength of the octupole magnetic field for instability suppression decreases. At the high energy stage, a field gradient of $K_3 \approx 20$ T/m$^2$ is necessary to completely mitigate instability. We set the target $K_3$ value to 45 T/m$^2$ at injection energy of $300\,\mathrm{MeV}$ (equivalent to 15 T/m$^2$ at extraction energy of $1.6\,\mathrm{GeV}$) to reduce the manufacturing complexity of the octupole magnets. The octupole strength in this design is insufficient to completely suppress the RCS instability on its own. Nevertheless, it is adequate when utilized alongside existing mitigation strategies. This integral magnetic field translates to a field gradient of $k_3 = 900$ T/m$^3$. TABLE 2 provides the main parameters of the octupole magnets and the power supply in the RCS. The octupole field switching is designed to be completed within $3\,\mathrm{ms}$, with a field change rate of less than $210$ T/m$^3$/ms.

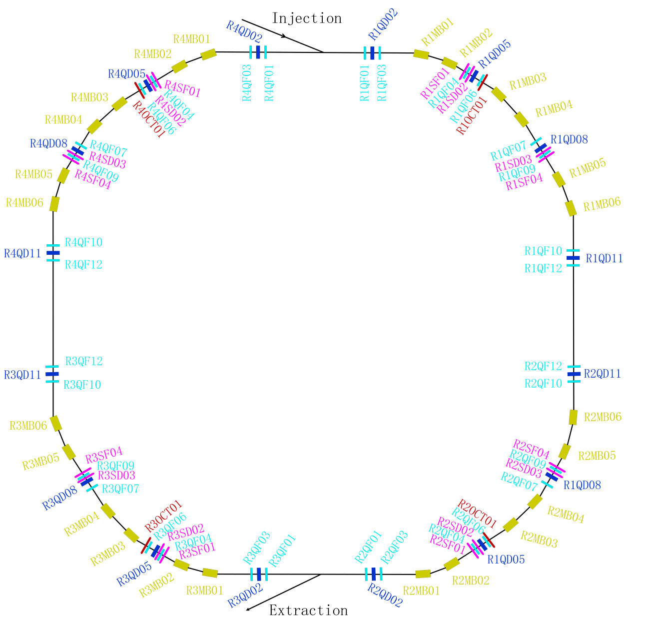


Fig. 3. (Color online) Magnet layout in the RCS, including four pulsed octupole magnets (dark red). The deep yellow, pink, cyan and blue denote dipole, sextupole, focusing and defocusing quadrupole magnets.

### A. Octupole magnet

The magnet, characterized by a core length of $0.2\,\mathrm{m}$ and a diameter of $256\,\mathrm{mm}$, is designed to match the physical aperture in the RCS. Fig. 4 displays full 3D diagram of octupole magnets and the 2D model with distribution of magnetic flux lines. The successful implementation of AC sextupole magnets [32] has provided valuable insights for the design and fabrication of pulsed octupole magnets. To enhance the mechanical rigidity of the magnet and facilitate the installation of the ceramic vacuum chamber, the pulsed magnet adopts an upper and lower half-in-one structure. The iron core is composed of $0.5\,\mathrm{mm}$ thick silicon steel insulated laminations, which are coated with B-stage epoxy resin. The end plate is constructed from stainless steel. The magnetic field is estimated after the pole chamfering, and the total high-order field error is less than 0.5%. The excitation curve calculations reveal that the nonlinearity of the integral magnetic field is less than 3%. Each magnet is powered individually. To mitigate the induced voltage caused by dynamic current, a 16-turn coil is selected, ensuring that the corresponding induced voltage of the power supply is within an acceptable level.

TABLE 2. Main parameters of octupole magnets and power supply in the RCS.

| Parameter [unit] | Value |
|---|---|
| Magnet number | 4 |
| Effective length [mm] | 200 |
| Maximum field gradient $k_3$ [T/m$^3$] | 900 |
| Changing rate of field gradient [T/m$^3$/ms] | 210 |
| Aperture [mm] | 256 |
| Good field radius [mm] | 118 |
| High-order-Field error [%] | $< 0.5$ |
| Self-inductance [mH] | 4.6 |
| Number of power supply | 4 |
| Maximum peak current [A] | 620 |
| Maximum peak voltage [V] | 740 |
| Changing rate of current [A/ms] | 130 |
| Current tracking error [%] | 3 |

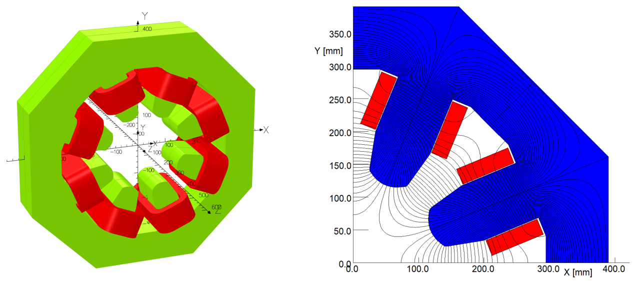

Fig. 4. (Color online) 3D diagram of octupole magnets (left) and 2D model with distribution of magnetic flux lines (right).

The primary objective of the dynamic magnetic field simulation is to compute the eddy current distribution and temperature rise within the iron core of the magnets. To enhance computational efficiency, a 1/8 core segment is utilized for analysis with the ELEKTRA/TR module in the OPERA software [33]. This approach enables the extraction of the magnetic field and other parameters at different excitation currents. A dedicated post-processing program is developed to process the calculation results. The average heat source density data obtained from the eddy current analysis is then imported into the TEMPO/ST module to calculate the temperature field, thereby determining the final temperature rise at various locations within the magnet core.

Following the setting of material constants and parameters, the dynamic magnetic field is simulated. Fig. 5 presents the reference curve of the magnetic field versus the excitation current in the simulation. Over a $40\,\mathrm{ms}$ period, 200 output points are obtained, with a convergence accuracy of $1 \times 10^{-3}$ using a reasonable mesh grid. The eddy current effects in the iron

core cause the magnetic field to change more slowly than the current, with a maximum time delay of approximately $0.2\,\mathrm{ms}$. The peak eddy current reaches $12\,\mathrm{A}$, corresponding to the maximum rate of change in the excitation current. After slotting the end plate, the maximum temperature rise recorded is around $50°\mathrm{C}$.

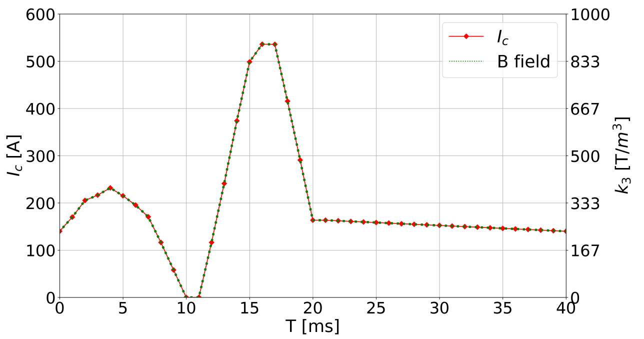


Fig. 5. (Color online) Designed curve of the magnetic field and excitation current for instability mitigation.

### B. Power supply

The octupole is powered individually by a programmable power supply, which is essential component in precision applications where high current and precise control are required. The maximum change rate is limited to $133\,\mathrm{A/ms}$, and corresponding to an excitation voltage of approximately $740\,\mathrm{V}$ considering the magnet inductance. The maximum current is $620\,\mathrm{A}$ to allow for a margin. The power supply system utilizes a standardized modular switch-mode design, achieving a total output of ±740V/±620A through the series connection of standardized power modules. It comprises a front stage, an isolation transformation circuit, and a back stage. The front stage employs a soft-switching parallel resonant circuit to minimize switching interference and noise. The isolation transformation circuit enhances the stability of the power supply. The back stage features an H-bridge chopper and an output filter, enabling bidirectional current and voltage output. With an equivalent switching frequency of approximately $60\,\mathrm{kHz}$, the system meets the demands for rapid magnetic field shutdown. The power supply achieves a target stability of $0.2\%$ and a current tracking accuracy of less than $3\%$. This level of stability ensures that the power supply can deliver a steady current over prolonged periods. The power supply is synchronized with the CSNS $25\,\mathrm{Hz}$ timing, ensuring alignment with dipole and octupole magnetic fields in the RCS. Additionally, the system includes comprehensive fault and protection functions to ensure operational safety.

## V. FIELD MEASUREMENT

Before the magnet installation into the RCS tunnel, a field measurement is conducted to evaluate the performance of the magnet system, including both static and dynamic field measurements. These measurements ensure that the magnetic field conforms to the design specifications, thereby preventing potential alignment and operational issues.

### A. Static field measurement

Static field measurements are performed to validate the physical design and manufacturing precision of the magnet. A Hall sensor [34] and a radial rotating coil [35] are employed in these measurements, utilizing a DC power supply. The repeatability of the Hall sensor is approximately $1\times10^{-4}$, while that of the radial rotating coil is better than $2 \times 10^{-4}$. The static magnetic field is measured up to $600\,\mathrm{A}$ in increments of $10\,\mathrm{A}$. Fig. 6 displays the measured excitation curve of the center field gradient. At an excitation current of $514\,\mathrm{A}$, the measured field is $900\,\mathrm{T/m^3}$. The maximum measured center field is $1021\,\mathrm{T/m^3}$ at $600\,\mathrm{A}$. The measured results are in good agreement with the calculated values. The effect of core saturation is negligible, and the field gradient is directly proportional to the excitation current $I$ with $k_3 = 1.751 \times I$. The effective length, derived from the measured center field gradient and the integrated field gradient, is $0.207\,\mathrm{m}$. Furthermore, the dispersion of the integral magnetic field among magnets is measured, and the result shows that the dispersion is less than $1.5\%$.

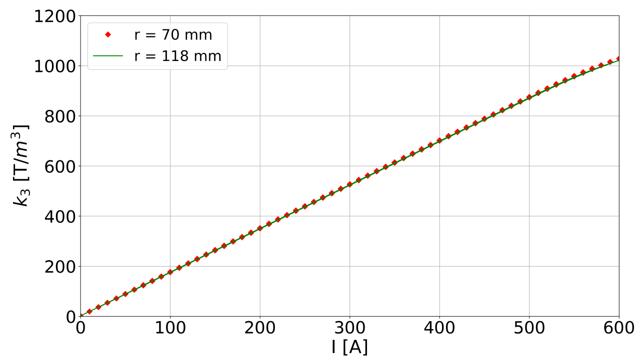


Fig. 6. (Color online) Excitation curve of the center octupole field gradient. The red diamond denotes the measured result at $r$ = $70\,\mathrm{mm}$, and the green line presents that at $r = 118\,\mathrm{mm}$.

### B. Dynamic field measurement

The purpose of the AC measurement of the magnets is to determine the dynamic response relationship between the current and the magnetic field, as well as the time delay induced by the excitation current waveforms. A stationary coil is utilized in the measurement. A timing clock is used to synchronize acquisition of the current signal and the induced voltage signal of the magnetic field. The coil coefficient is calibrated using the Hall measurement results to enhance measurement accuracy and obtain the absolute value of the integral mag-

netic field. During the measurement, the magnet is first powered by a sinusoidal current to heat and reach a thermally stable state in about 2 hours. Fig. 7 displays the excitation current and integral magnetic field curves corresponding to the reference waveform in Fig. 5, where only the beam acceleration period is presented. The magnetic field changes almost synchronously with the current curve, with a time delay of approximately $0.2\,\mathrm{ms}$ during the acceleration cycle. Additionally, different excitation current waveforms are employed, including triangular, trapezoidal, and sine waves. The maximum time delay recorded is around $0.3\,\mathrm{ms}$. The repeatability for a given waveform is $0.1\%$.

Through these rigorous measurements, the octupole magnet and its corresponding power supply have demonstrated remarkable precision and stability. Consequently, we conclude that the magnet system complies with the design specifications, providing essential data support for subsequent applications in the RCS.

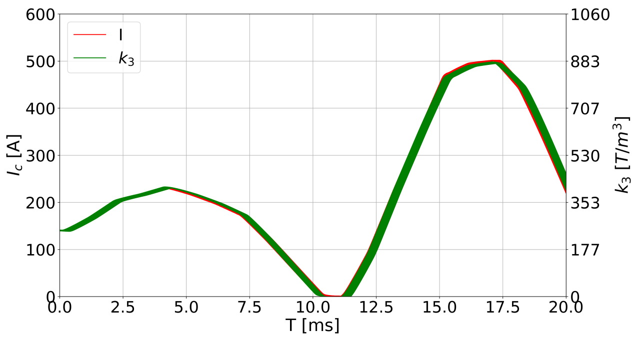


Fig. 7. (Color online) The response of the integrated magnetic field gradient to the excitation current over 30 trials. The red lines represent the excitation currents, and the green lines represent the integrated magnetic field gradients.

## VI. BEAM MEASUREMENT OF THE INSTABILITY

Following the installation of the magnets, a beam test with the octupole field is promptly conducted. Initially, critical magnetic field measurements with the beam are executed, including magnetic field alignment and synchronized measurements with the RCS timing. Subsequently, extensive measurements for instability mitigation are conducted. The tunes play a significant role in impacting the instability. The TbT bunch position is analyzed for the observed instability covering the entire ramping process. The total number of particles is $N_p = 2.2 \times 10^{13}$ per pulse, corresponding to a beam power of $140\,\mathrm{kW}$. Fig. 8 shows measured beam positions and beam populations with and without the optimized octupole field curve, including horizontal tunes of 4.80, 4.86, and 4.90, respectively. The oscillation amplitudes at the three distinct horizontal tunes display considerable variation as shown in Figs. 8 (b), (c), and (d). When the octupole magnet is off, instabilities are observed for all tunes. With the optimized octupole field curve for different tunes in Fig. 8(a), the instability can be entirely suppressed by the optimized field curve for all tunes, and the transmission efficiency is also enhanced in the acceleration cycle. The results of this test confirm that the octupole magnet is effective in suppressing the RCS instability, as predicted.

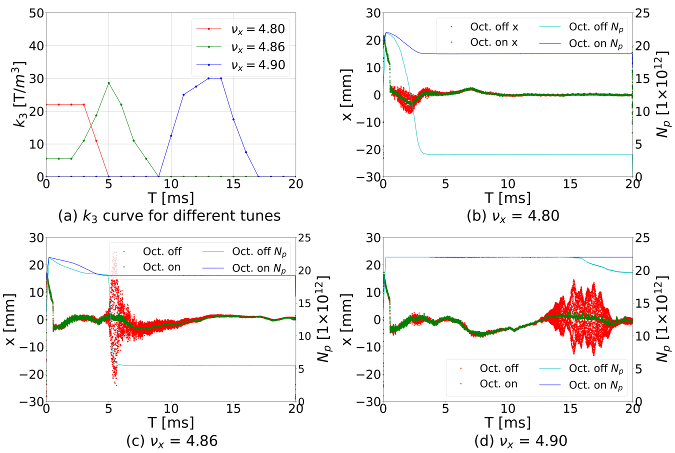


Fig. 8. (Color online) Experimental results of octupole magnet mitigation of instabilities at different timings. (a) is the applied $k_3$ curves for different tunes. The TbT bunch positions and beam populations with and without the field curve depicts for horizontal tune of 4.80 (b), 4.86 (c) and 4.90 (d), respectively.

In the operational tune with $\nu_x = 4.80$, the instability is successfully suppressed through chromaticity optimization [17]. Following this, we increased the octupole magnet strength to examine its impact on the beam. As illustrated in Fig. 9, with an optimized curve on the left, the octupole magnets further improved the RCS transmission efficiency on the right, which was not anticipated in the initial design. The octupole magnet strength applied is very weak, with $k_3 \approx 1$ T/m$^3$, as depicted in the left panel. We propose that this enhancement is due to the compensatory effects of the octupole magnets on the nonlinearities in the RCS. As a result, octupole magnets have been employed in subsequent operations to boost the transmission efficiency.

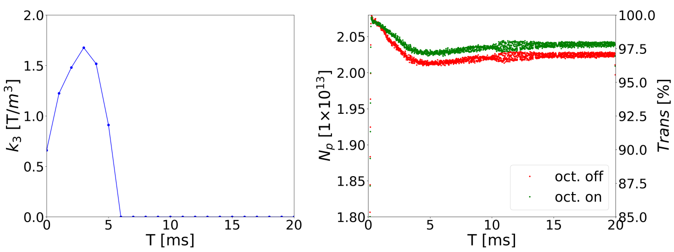


Fig. 9. (Color online) The RCS transmission efficiency (right) with and without the octupole field curve (left) in the operation. The instability is fully suppressed through chromaticity optimization in this case.

In the RCS, space charge effects are predominant during the low energy phase, especially before $5\,\mathrm{ms}$. As the beam energy increases, the space charge effects diminish. Accord-

ing to existing literature [36], the strength of octupole magnets required to suppress instabilities increases significantly under strong space charge effects. For a bunched beam, the dynamics influenced by nonlinearities due to octupoles are complex, and thus Landau damping cannot be adequately described by simplified dispersion relations [37]. This complexity is addressed in our study through detailed measurements. As shown in Fig. 8, the instability is observed at different times depending on the tune. Instability is observed at the low energy stage where space charge effects are strong at $\nu_x = 4.80$. Conversely, instability is observed at the high energy stage with weak space charge effects at $\nu_x = 4.90$. This scenario allows for an experimental comparison of the impact of space charge effects on the coupled bunch instability. By setting the tunes to $\nu_x = 4.80$ and $\nu_x = 4.90$ at a beam power of $140\,\mathrm{kW}$, and adjusting beam parameters to induce strong horizontal oscillations, the octupole magnet strength is then incrementally increased to mitigate the instability until it is fully suppressed. The growth times of instabilities and the corresponding octupole strengths are summarized in TABLE 3. Proportional calculation indicates that $k_3 = 8.4$ is required to suppress the instability with a growth time of $3.2\,\mathrm{ms}$ at $\nu_x = 4.80$. Compared to the instability occurring under weak space charge effects, the required octupole field strength significantly increases for RCS instability mitigation under strong space charge effects in TABLE 3.

TABLE 3. Growth time and required octupole strength to mitigation the RCS instability at different tunes.

| parameter [unit] | value | value |
|---|---|---|
| $\nu_x$ | 4.80 | 4.90 |
| Instability observed time [ms] | 2 | 14 |
| Space charge tune shift | 0.27 | 0.006 |
| Growth time [ms] | 3.2 | 4.5 |
| $k_3$ | 16 | 6 |

## VII. DISCUSSION

In the CSNS/RCS, octupole magnets have shown excellent performance in suppressing instability at the high energy stage (approximately after $10\,\mathrm{ms}$). They achieve complete suppression of the instability and maintain a 100% transmission efficiency, thus meeting the requirements for long-term stable operation of the accelerator. Despite the effectiveness of octupole magnets in suppressing instabilities and improving transmission efficiency at the low energy stage, the RCS transmission efficiency remains inadequate for meeting operational demands (about 10% loss in Fig. 8). This is evident for the tunes of 4.80 and 4.86 in Fig. 9. At present, chromaticity optimization is primarily used to suppress instability and achieve high RCS transmission efficiency during operation. Based on this, we performed tests to assess the impact of octupole magnets on transmission efficiency. The results showed that as the strength of the octupole magnets increased, the transmission efficiency progressively decreased. An energy deviation for the RCS beam at injection is introduced to mitigate the space charge effects [38]. The maximum momentum shift $\Delta p/p$ is close to 1%. To address the transmission efficiency issue, we performed a detailed analysis, including the $2^{nd}$ chromaticity effects and dynamic aperture.

The octupole magnet is placed in the arc with dispersion function $D_x \approx 4.0$ meters and the tune shift due to the $2^{nd}$ order chromaticity [39] is expressed as

$$\Delta\nu = \frac{1}{8\pi} k_3 \beta D_x (\Delta p/p)^2, \tag{10}$$

with the beta function $\beta$. The $2^{nd}$ chromaticity in the vertical plane is measured using the pulsed octupole magnet. The vertical tune is determined by acquiring the TbT bunch position. An extraction kicker [40] is implemented to induce a visible oscillation in the vertical plane, providing better accuracy compared to the designed tune excitation [41]. Typically, tune measurements are conducted over 1024 turns at $11\,\mathrm{ms}$, and the timing of the vertical kicker can be adjusted to the moment of interest. The $2^{nd}$ chromaticity is determined by fitting the tunes versus the momentum shift, which is controlled by modulating the RF frequency. The measurement is carried out at a low beam power of $20\,\mathrm{kW}$. Fig. 10 presents the measured tunes with and without the octupole field at different momentum shifts. For each momentum shift, measurements are taken five times. A box plot is provided to visualize the raw data, and the median difference for the two cases is fitted to determine the $2^{nd}$ chromaticity. With the momentum deviation $\Delta p/p$, the tune shift is inferred as $\Delta\nu_y \approx 10 \cdot (\Delta p/p)^2$. Notably, only the designed white noise excitation is used to measure the tune in the RCS. The $2^{nd}$ chromaticity in the horizontal plane is not measured due to poor measurement accuracy with this white noise. Given similar horizontal and vertical beta functions at the octupole magnet, the $2^{nd}$ chromaticity in the horizontal plane is approximately assumed to be equal to that in the vertical plane. Based on this calculation, the maximum tune shift due to the $2^{nd}$ chromaticity in the RCS is approximately 0.001, which is significantly smaller than the space charge tune shift of 0.3 [42]. Consequently, the beam loss due to the $2^{nd}$ order chromaticity can be ignored.

Utilizing a simplified lattice at a constant energy of $80\,\mathrm{MeV}$, we perform a comprehensive calculation of the dynamic aperture at various energy deviations, as depicted in Fig. 11. Chromaticity correction is implemented using the sextupole magnet. The case of only chromaticity correction (a) and the case of only an octupole field (c) are also presented for comparison. In the horizontal plane, the dynamic aperture is larger than the physical aperture of $60\,\mathrm{mm}$ for the case of only chromaticity correction (a), achieving a beam transmission efficiency of approximately 100% in actual operation. However, the dynamic aperture significantly diminishes with octupole fields. The dynamic aperture notably decreases for the case of only an octupole field (c), particularly for the case of additional chromaticity correction (b). At the low energy stage, both the beam size and momentum spread are relatively large. Under these conditions, even a weak octupole field may induce beam loss. As the beam energy increases, the beam size and momentum spread decrease. At the high energy stage, the beam can sustain stability even with a stronger

octupole field. Consequently, it is essential to increase the dynamic aperture, thereby improving the RCS transmission efficiency at the low energy stage. A viable approach to restoring the RCS transmission efficiency is to relocate the octupole magnets, a subject of our ongoing research.

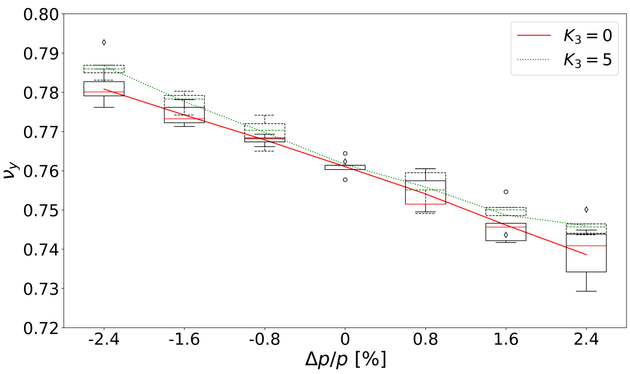


Fig. 10. (Color online) Measured tune in term of momentum shift with and without octupole magnet, where the red solid line represents the median line when the magnet OFF, while the green dashed line indicates that when the magnet ON.

## VIII. CONCLUSION

The coupled bunch instability has been observed in the RCS of the CSNS. As power levels increase in CSNS-II, more methods for suppressing this instability are being explored. One such method involves the use of octupole magnets to provide Landau damping. The pulsed octupole magnet system has been developed in the RCS. One octupole magnet is accommodated in every super-period to preserve the lattice symmetry and efficiently use the existing ceramic chambers. Field measurements confirm that the magnet satisfies the design values. After the installation of the magnet, preliminary measurements of the instability are performed. The instability is successfully suppressed by implementing the designed pulsed octupole magnets. At the high energy stage, the instability can be fully suppressed using the pulsed octupole magnet without any additional beam loss, thereby meeting the requirements for long-term stable operation of the CSNS. However, at the low energy stage, although the octupole magnet effectively suppresses the instability, the RCS transmission efficiency still falls short of operational conditions. This may be attributed to the reduction in dynamic aperture, necessitating further optimization to improve transmission efficiency, including the relocation of octupole magnets. Moreover, when the instability is completely suppressed through chromaticity optimization, octupole magnets can significantly enhance the RCS transmission efficiency, which is crucial for controlling beam loss during the current operations of the CSNS. More detailed measurements on instability mitigation should be carried out in future machine studies. Nevertheless, significant advancement in beam stability has been made in the preliminary measurements, providing valuable experience for further beam power enhancement.

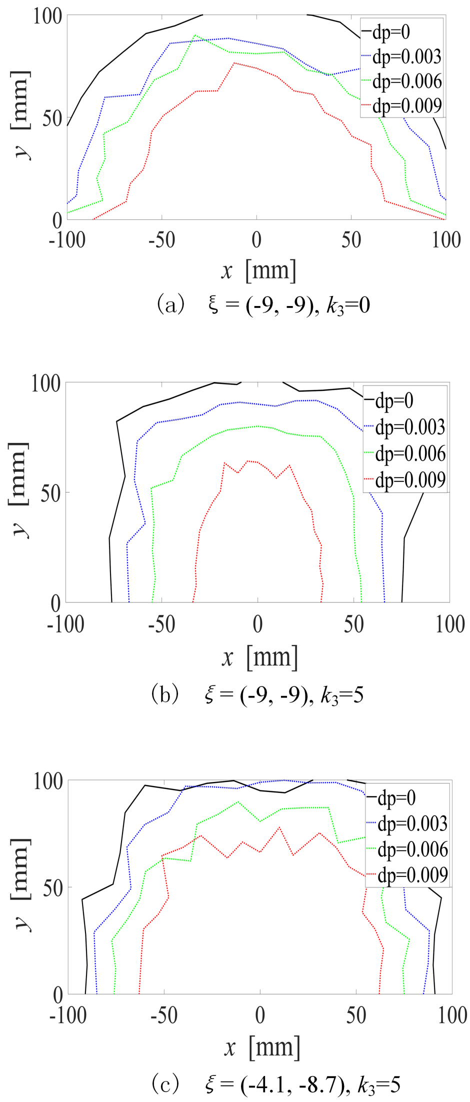


Fig. 11. (Color online) The dynamic aperture in term of $\Delta p/p$ (dp), where the tune is (4.80, 4.86) with constant energy of 80 MeV. (a) is optimized chromaticity and octupole off, (b) is optimized chromaticity of (-9, -9) and $k_3$ = 5, and (c) is natural chromaticity and $k_3$ = 5.

## ACKNOWLEDGEMENTS

We extend our sincere gratitude to our colleagues in the Physics Group, the Magnet Group, the Power Supply Group, and the Mechanical Group of CSNS for their substantial support in the magnet design and field measurement. We also wish to thank our colleagues in the Beam Diagnosis and Operation Groups for their invaluable assistance during beam measurements. This work is supported by the Guangdong Basic and Applied Basic Research Foundation, China (Project: 2021B1515140007).

[1] T. Miyajima, Y. Kobayashi, S. Nagahashi, Development of a pulsed octupole magnet system for studying the dynamics of transverse beam instabilities in electron storage rings. Nucl. Instrum. Methods Phys. Res. A. **581**, 589-600 (2007). doi: 10.1016/j.nima.2007.08.120

[2] S. Igarashi, A. Ando, T. Koseki, Octupole magnets for the instability damping at the J-PARC main ring. In Proc. of IPAC'12, New Orleans, Louisiana, USA, WEPPR052, 3045-3047 (2012).

[3] X. Buffat, W. Herr, N. Mounet, et al., Stability diagrams of colliding beams in the Large Hadron Collider. Phys. Rev. Accel. Beams **17**, 111002 (2014). doi: 10.1103/PhysRevSTAB.17.111002

[4] P. Spiller, U. Blell, L. Bozyk, et al., Status of the FAIR Heavy Ion Synchrotron Project SIS100. In Proc. of IPAC'15, Richmond, VA, USA, THPF015, 3715-3717 (2015). doi: 10.18429/JACoW-IPAC2015-THPF015

[5] Q. Qin, Z. Guo, H. Huang, et al., Electron cloud instability experiments on the BEPC. Nucl. Instrum. Methods Phys. Res. A. **547**, 239-248 (2005). doi: 10.1016/j.nima.2005.02.027

[6] S. Y. Lee, Accelerator Physics $2^{nd}$ ed. World Scientific, Singapore, 64 (2004).

[7] S. Wang, S. X. Fang, S. N. Fu et al., Introduction to the overall physics design of CSNS accelerators, Chinese Physics C **33(S2)**, 1-3 (2009). doi: 10.1088/1674-1137/33/S2/001

[8] Y. Shi, M. Zhang, L. Ou-Yang., et al. Design of a rapid-cycling synchrotron for flash proton therapy. NUCL SCI TECH. **34**, 145 (2023). doi: 10.1007/s41365-023-01283-3

[9] China Spallation Neutron Source. Available at http://english.ihep.cas.cn/csns, date last accessed July 24, 2024.

[10] J. Wei, H. S. Chen, Y. W. Chen, et al., China Spallation Neutron Source: Design, R&D, and outlook, Nucl. Instrum. Methods Phys. Res. A. **600**, 10–13 (2008). doi: 10.1016/j.nima.2008.11.017

[11] H. Liu, J. Peng, K. Gong, et al., The design and construction of CSNS drift tube linac. Nucl. Instrum. Methods Phys. Res. A. **911**, 131-137 (2018). doi: 10.1016/j.nima.2018.10.034

[12] J. Peng, Y. Han, Z. Li, et al., Beam dynamics studies for the CSNS due to a quadrupole fault. In Proc. of LINAC'18, Beijing, China, TUPO114, 573-575 (2018). doi: 10.18429/JACoW-LINAC2018-TUPO114

[13] J. Peng, Y. Han, Z. Li, et al., Beam loss studies in the CSNS Linac. In Proc. of HB'23, Geneva, Switzerland, WEA4C1, 297-299 (2023). doi: 10.18429/JACoW-HB2023-WEA4C1

[14] S. Wang, S. Fu, H. Qu, et al., Development and Commissioning for High-intensity Proton Accelerator of China Spallation Neutron Source, Atomic energy science and technology **56(9)**, 1747-1759 (2002). doi: 10.7538/yzk.2022.youxian.0591

[15] S. Xu, H. Liu, J. Peng, et al., Beam commissioning and beam loss control for CSNS accelerators, JINST **15**, P07023 (2020). doi: 10.1088/1748-0221/15/07/P07023

[16] L. Huang, S. Xu, S. Wang, The characteristic of the beam position growth in CSNS/RCS, In Proc. of IPAC'21, Campinas, Brazil, TUPAB262, 630–632 (2021). doi: 10.18429/JACoW-IPAC2021-TUPAB262

[17] L. Huang, Y. An, C. Deng, et al., Upgrade of the sextupole field for beam instability mitigation in rapid cycling synchrotron of China Spallation Neutron Source. Radiat. Detect. Technol. Methods **7**, 550-560 (2023). doi: 10.1007/s41605-023-00428-7

[18] Y. Li, Y. Yuan, S. Xu, et al., Half-integer resonance caused by dc injection bump magnets and superperiodicity restoration in high-intensity hadron synchrotrons. Phys. Rev. Accel. Beams **26**, 104201 (2023). doi: 10.1103/PhysRevAccelBeams.26.104201

[19] B. Wu, X. Li, Z. Li, et al., Development of a large nanocrystalline soft magnetic alloy core with high $\mu_p'$Qf products for CSNS-II. NUCL SCI TECH **33**, 99 (2022). doi: 10.1007/s41365-022-01087-x

[20] J. Wu, X. Li, B. Wu, et al. Design and commissioning of a wideband RF system for CSNS-II rapid-cycling synchrotron. NUCL SCI TECH **35**, 5 (2024). doi: 10.1007/s41365-022-01087-x

[21] H. Liu, S. Wang, Longitudinal beam dynamic design of 500 kW beam power upgrade for CSNS-II RCS. Radiat. Detect. Technol. Methods **6**, 339-348 (2022). doi: 10.1007/s41605-022-00325-5

[22] L. Huang, M. Huang, S. Xu, et al., Intense Beam Issues in CSNS Accelerator Beam Commissioning. In Proc. of HB'23, Geneva, Switzerland, MOA1I3, 16-22 (2023). doi: 10.18429/JACoW-HB2023-MOA1I3

[23] L. Huang, S. Wang, S. Xu, et al., Sourceof instability in the rapid cycling synchrotron of the China Spallation Neutron Source, Eur. Phys. J. Plus **140(1)**, 71 (2025). doi: 10.1140/epjp/s13360-025-05997-8

[24] H. Dong, H. Song, Q. Li, et al., The vacuum system of the China spallation neutron source, vacuum **154**, 75-81, (2018). doi: 10.1016/j.vacuum.2018.04.046

[25] D. Mohl, H. Song, Q. Li, et al., On Landau Damping of dipole modes by nonlinear space charge and octupoles, Part. Acc. **50**, 177-187, (1995).

[26] J. Gareyte, J. P. Koutchouk, F. Ruggiero, Landau damping, dynamic aperture and octupoles in LHC, CERN-LHC-Project-Report-91, (1997).

[27] K. Y. Ng, Physics of Intensity Dependent Beam Instabilities. World Scientific, Singapore, (2006).

[28] A. W. Chao, Physics of Collective Beam Instabilities in High Energy Accelerators. Wiley, New York, 15 (1993).

[29] L. Huang, Y. Liu, S. Wang, Resistive wall instability in rapid Cycling synchrotron of China spallation neutron source. Nucl. Instrum. Methods in Phys. Res., Sect. A. **728**, 1-5, (2013). doi: 10.1016/j.nima.2013.06.017

[30] S. Xu, S. Wang, Study of eddy current power loss in an RCS vacuum chamber, Chinese Physics C **36(2)**, 160-166 (2012). doi: 10.1088/1674-1137/36/2/011

[31] S. Wang, Y. An, S. Fang, et al., An overview of design for CSNS/RCS and beam transport. Sci. China Phys. Mech. Astron. **54(S2)**, 239–244 (2011). doi: 10.1007/s11433-011-4564-x

[32] C. Deng, Y. Liu, X. Wu, et al., Transient Simulation and Field Measurement of the Trim Quadrupoles and AC Sextupoles for CSNS/RCS Upgrade. IEEE transactions on applied superconductivity **32(6)**, 4002605 (2022). doi: 10.1109/TASC.2022.3151577

[33] OPERA code, Available at https://www.3ds.com/products/simulia/opera, date last accessed July 29, 2024.

[34] X. Wu, W. Kang, W. Chen, et al., Design and performance of hall probe measurement system in CSNS. Radiat. Detect. Technol. Methods **1(18)**, 1-5 (2017). doi: 10.1007/s41605-023-00428-7

[35] J. Zhou, W. Kang, S. Li, et al., Development of rotating coil measurement system for China spallation neutron source. High Power Laser Part. Beams **30(10)**, 105101 (2018). doi: 10.11884/HPLPB201830.180186

[36] V. Kornilov, O. Boine-Frankenheim, Landau damping due to octupoles of non-rigid head–tail modes. Nucl. Instrum. Methods in Phys. Res., Sect. A. **951**, 163042 (2020). doi: 10.1016/j.nima.2019.163042

[37] V. Kornilov, O. Boine-Frankenheim, Space charge effects on Landau damping from octupoles, In Proc. of the ICFA mini-Workshop MCBI'19, Zermatt, Switzerland, 237-241 (2019).

[38] L. Huang, H. Liu, M. Li, et al., Longitudinal dynamics study and optimization in the beam commissioning of the rapid cycling synchrotron in the China Spallation Neutron Source. Nucl. Instrum. Methods in Phys. Res., Sect. A. **998**, 165204 (2021). doi: 10.1016/j.nima.2021.165204

[39] V. H. Ranjbar, C. Y. Tan, Effect of impedance and higher order chromaticity on the measurement of linear chromaticity. Phys. Rev. Accel. Beams **14**, 082802 (2011). doi: 10.1103/PhysRevSTAB.14.082802

[40] W. Kang, L. Wang, L. Huo, et al., Design and prototype test of CSNS/RCS injection and extraction magnets. IEEE tran. on appl. sup. **20(3)**, 356-359 (2010). doi: 10.1109/TASC.2010.2041756

[41] X. Yang, T. Xu, S. Fu, Classical and modern power spectrum estimation for tune measurement in CSNS RCS, Chinese Physics C **36(7)**, 666-669 (2013). doi: 10.1088/1674-1137/37/11/117003

[42] S. Xu, S. Fang, S. Wang. Study on space charge effects of the CSNS/RCS, In Proc. of ICAP'09, San Francisco, CA, USA, TH4IODN04, 239-244 (2009).